Automatic alignment of myocardial perfusion PET and 64-slice coronary CT angiography on hybrid PET/CT

Ryo Nakazato, MD, PhD[a], **Damini Dey, PhD**[b,c], **Erick Alexánderson, MD**[d,e], **Aloha Meave, MD**[d,e], **Moisés Jiménez, MD**[d,e], **Edgar Romero, MD**[d], **Rodrigo Jácome, MD**[d], **Marco Peña, MD**[d], **Daniel S. Berman, MD**[a,c], and **Piotr J. Slomka, PhD**[a,c]

[a]Departments of Imaging and Medicine, and Cedars-Sinai Heart Institute, Cedars-Sinai Medical Center, Los Angeles, CA, USA

[b]Department of Biomedical Sciences and Biomedical Imaging Research Institute, Cedars-Sinai Medical Center, Los Angeles, CA, USA

[c]David Geffen School of Medicine, University of California Los Angeles, Los Angeles, CA, USA

[d]Unidad PET/CT Ciclotrón, Facultad de Medicina, Universidad Nacional Autónoma de México, Mexico, D.F., Mexico

[e]Instituto Nacional de Cardiología Ignacio Chávez, Mexico, D.F., Mexico

Abstract

Background—Hybrid PET/CT allows acquisition of cardiac PET and coronary CT angiography (CCTA) in one session. However, PET and CCTA, are acquired with differing breathing protocols and require software registration. We aimed to validate automatic correction for breathing misalignment between PET and CCTA acquired on hybrid scanner.

Methods—Single-session hybrid PET/CT studies of rest/stress ^{13}N-ammonia PET and CCTA in 32 consecutive patients were considered. Automated registration of PET left ventricular (LV) surfaces with CCTA volumes was evaluated by comparison to expert manual alignment by 2 observers.

Results—The average initial misalignment between the position of LV on PET and CCTA was 27.2±11.8mm, 13.3±11.5mm, and 14.3±9.1mm in x, y, and z axes on rest, and 26.3±10.2mm, 11.1±9.5mm, and 11.7±7.1mm in x, y, and z axes on stress. The automated PET-CCTA co-registration had 95% agreement as judged visually. Compared to expert manual alignment, the translation errors of the algorithm were 5.3±2.8mm (rest) and 6.0±3.5mm (stress). 3D visualization of combined coronary vessel anatomy and hypoperfusion from PET could be made without further manual adjustments.

Conclusion—Software co-registration of CCTA and PET myocardial perfusion imaging on hybrid PET/CT scanners is necessary, but can be performed automatically, facilitating integrated 3D display on PET/CT.

Address for correspondence: Piotr Slomka, PhD, Department of Imaging, Cedars-Sinai Medical Center, 8700 Beverly Boulevard, Taper Building Suite A047, Los Angeles, CA 90048, USA, Phone: 310-423-4348, Fax: 310-423-0171, slomkap@cshs.org.

Conflict of interest statement:

Drs. Daniel Berman and Piotr Slomka receive royalties from the software employed in the study. All others disclose no current conflict of interest.

INTRODUCTION

Both myocardial perfusion imaging (MPI) and coronary CT angiography (CCTA) are widely used for assessment of patients with suspected or known coronary artery disease (CAD). In current clinical practice, a physician subjectively performs the integration of anatomic and physiologic information from angiography and MPI. The two image sets are viewed independently, and integration of the information is performed mentally. Some proportion of patients requires both examinations because of inconclusive results obtained by the first test.(1, 2) In such cases, the combined imaging results are often challenging to interpret, because of the presence of artifacts or equivocal findings in at least one modality. In addition, the location of a stenosis with respect to the left ventricular epicardial surface can only be judged with considerable approximation in some cases. The existence of more than one stenosed artery exacerbates this problem, especially if the degree of stenosis is unclear since such stenosis may or may not cause perfusion abnormalities.

It has been suggested that visual analysis of fused MPI and CCTA images can synergistically improve the diagnostic value of sequential combined imaging and reduce the rate of equivocal studies.(3, 4) Manual tools for the purpose of combined visual analysis have been developed.(5) However, the manual interactive alignment of the images from two modalities introduces subjective errors, takes a substantial amount of time, and limits the practical clinical use of such tools. Previously, automated software tools for registering standalone single photon emission computed tomography (SPECT)-MPI and CCTA (6, 7) and SPECT to magnetic resonance imaging (8) have been described.

Hybrid positron emission tomography (PET)/CT potentially allows integrated multimodality cardiac evaluation of MPI and CCTA in one scanning session. However, even with the hybrid scanner, the PET and CCTA are not truly simultaneous and are acquired with differing breathing protocols, resulting in significant misalignments of the images from the two modalities. Subsequently, cardiac PET and CCTA images cannot be accurately fused by hardware registration alone.

The aim of this study was to evaluate the amount of initial misalignment that occurs between cardiac PET and CCTA studies obtained in one session on a hybrid scanner and to determine whether previously developed software for standalone SPECT-CCTA cardiac applications(6) could be applied as an automated correction tool for breathing misalignment between CCTA and cardiac PET.

METHODS

Patient Population

The study population consisted of a consecutive 32 patients (21 men, age 62 ± 9 years) with suspected CAD referred for combined clinical evaluation of myocardial ischemia and coronary anatomy in the same setting (Table 1). Seventeen patients had chest pain and 9 patients had dyspnea. Patients with known hypersensitivity to the substances used during the study (i.e. β-blockers, iodinated contrast agent), patients with renal failure (serum creatinine level >1.2mg/dL), and patients with contraindications for adenosine administration were all excluded. The study was approved by the Institutional Review Board.

Integrated PET-CT Imaging

All patients were studied on a whole-body 64-slice PET/CT scanner (Biograph-64 TruePoint PET/CT; Siemens Medical, Erlangen, Germany). Patients were studied after an overnight

fast, and all refrained from caffeine-containing beverages or theophylline-containing medications for 24 h prior to the study.

¹³N-ammonia PET scan acquisition, reconstruction—All image data was acquired in list mode. Myocardial perfusion was assessed at rest and during vasodilator stress with adenosine and with ¹³N-ammonia as a tracer. Two CT-based transmission scans (120 kVp; 20–30 mA; pitch = 1.35) were obtained prior to the rest perfusion studies and after the stress perfusion studies, for soft tissue photon attenuation. Myocardial perfusion was first assessed during rest using 20 mCi of ¹³N-ammonia. Rest imaging extended for 10 min and started few seconds before the ¹³N-ammonia injection. The ¹³N-ammonia was administered as a single peripheral IV bolus (3–5 s), followed by a 10-ml saline flush. Thirty min later a stress scan was performed, beginning with the infusion of adenosine over a 6-min period (0.14 mg/kg/min). A second dose of 20 mCi of ¹³N-ammonia was injected at the third min of the adenosine infusion, with 10 min stress acquisition started few seconds before the radiotracer injection. Patients were instructed to breathe normally during the CT transmission and PET acquisition. The estimated mean effective radiation dose from ¹³N-ammonia PET was 1.5 mSv for both rest and stress.(9) Static images were generated from the list mode data using standard reconstruction (2D Attenuation Weighted Ordered Subsets Expectation Maximization) with 3 iterations and 14 subsets and 3D post-filtering with 5mm Gaussian kernel. Transverse data was reformatted to 168×168×47 matrix with 2 mm pixel size. Static stress and rest perfusion images were reconstructed from the list mode data with a delay of 2 minutes to allow for the clearance of the radioactivity from the blood pool.

CCTA scan acquisition, reconstruction and interpretation—CCTA (64-slice) was performed immediately after completion of the rest-stress ¹³N-ammonia PET protocol, without changing patient position on the imaging table. Prior to CT imaging, patients with a heart rate >70 bpm were given metoprolol (up to 100 mg oral or 20 mg intravenous in 5 mg increments) to attain a heart rate <70 bpm. A short-acting nitrate (5 mg of isosorbide dinitrate) was given to all patients 2–3 min prior to the scan. For CCTA, after a timing bolus, ECG gated helical scanning was performed using ECG-based dose modulation whenever possible, and administration of 60 to 80 mL of Iopamiron 370 (370 mg iodine/mL, rate 5 mL/sec, Schering Bayer, Germany) during a single breath-hold (~10 sec). Scan parameters included heart rate dependent pitch (range, 0.18–0.2), 330-ms gantry rotation time, 120-kVp tube voltage, 550–945 mA tube current. The estimated mean effective radiation dose ranged from 12–15 mSv. Retrospectively, gated reconstruction of contrast-enhanced data was performed at end-systole and in diastole with the use of the following parameters: 0.6 mm slice thickness, 0.3 mm slice increment, 250 mm field of view, 512×512 matrix, and a "medium smooth" kernel. The cardiac phase with the best image quality was used for further analysis. All CCTA images were analyzed by an experienced cardiologist blinded to the MPI scan result. Luminal-diameter stenosis severity was assessed as recommended stenosis grading.(10) Percent obstruction of coronary artery lumen was based on a comparison of the luminal diameter of the segment exhibiting obstruction to the luminal diameter of the most normal-appearing site immediately proximal to the stenotic lesion. Obstructive stenosis was defined as   50% luminal stenosis by visual assessment.

Myocardial perfusion quantification—The quantitative perfusion variable employed was total perfusion deficit (TPD), which reflects a combination of both extent and severity of the defect in one parameter, as previously described.(11) Stress, rest and reversible (difference between stress and rest) myocardial perfusion defects on PET/CT were assessed by quantification of the TPD.(12, 13) MPI analysis was performed individually for each vessel with the "group" function in QPET, in which 17 segments are assigned to a vascular territory on the basis of the perfusion-defect pattern.(11) The portion of the TPD

corresponding to a given territory was used for the automated quantification in each vessel, with a threshold of 2% as previously established.(11, 14) We have used the ^{13}N-ammonia normal limits database, which is derived from gender combined very low likelihood patients with normal perfusion images, for perfusion quantification.(15)

Automated co-registration—We have adopted previously developed software for standalone SPECT to CCTA registration.(6) Briefly, to provide a robust registration approach, we registered pre-segmented MPI volumes using the left ventricle (LV) segmentation algorithm of quantitative gated PET(16) and the additional segmentation of the blood-pool region, derived from the MPI LV definition. For both CCTA and MPI, transverse image orientation was used during the registration process. The MPI-CCTA registration algorithm was implemented as previously described.(6) Phase adjustment as previously described(7) was not performed in the current study. Automated co-registration was performed without any manual intervention. An overview of image processing is presented in Figure 1.

Manual co-registration—For validation purposes, separate expert manual alignment was performed without knowledge of the automated co-registration results. Two expert observers independently verified the alignment of CCTA images with emission PET data, using the fusion capability of the quantitative perfusion QPET software developed at our institution. (14) Data were reviewed in all planes using a multiplanar (sagital, coronal, and transverse) display of PET, CT, and fused PET/CT data. The manual alignment parameters [3 translations (x, y, z)] by expert observers were recorded for the comparison with the automated co-registration. X axis reflects left to right direction, y axis reflects front to back direction, z axis reflects bottom to top (feet to head) direction. Experts were able to adjust the window and level settings on the CT display and adjust alpha-blending between PET and CT image components before adjusting the position. Roving window display (an interactive superimposition of a portion of the PET image on the CT image) was also used in all cases to judge the misalignment.(17) The observers performed a visual alignment in 3 dimensions (x, y, z), adjusting x, y, and z shifts to measure quantitatively the misalignment between PET and CCTA data. The manual alignment process took about 2–3 min for each case. To resolve the differences between 2 observers for the misalignment correction, average x, y, and z misalignments were computed by averaging 2 observers' results for each case.

Comparison of manual and automatic registration—The automated co-registration algorithm was applied and compared to the average visual alignment for the 64 datasets (32 stress and 32 rest). The offset from mean observer location choice was defined based on the comparison of automated co-registration with averaged manual registration by 2 observers as the difference between the results of manual and automated alignment. The initial misalignment between PET and CCTA before any corrections were applied (amount of motion correction) was defined as the difference between alignment parameters before and after automated co-registration as well as before and after manual registration.

Vessel extraction and 3D visualization—For the 3D visualization of coronary vessels superimposed with MPI surfaces, we used the output obtained from CCTA analysis using the Syngo Circulation software (Siemens, Erlangen, Germany) on a LEONARDO workstation (Siemens, Forchheim, Germany). The coronary tree was segmented automatically with a region-growing algorithm. To complete the coronary artery tree, missing vessel segments were marked manually and then added to the data set by the algorithm.(18) The computer file containing the 3D binary mask was transferred to the standalone workstation with QPET software. Within QPET, volume rendering was performed in OpenGL with 2D/3D textures and pre-assigned color tables with varying red-

green-blue intensities and opacities to maximize the contrast opacity, provide realistic display (blood/tissue, pink/red; calcium, white), and minimize the influence of neighboring tissue such as fat.(19) Further details were previously described.(6) A 3D bounding box was used to speed up the volume rendering of coronary arteries. The bounding box was directly computed from the coronary mask. The rendering was integrated with the standard 3D MPI epicardial surfaces. Raw perfusion information of quantitative blackout maps could be displayed on the epicardial surface. Stress and rest images had the same CCTA image superimposed. These segmented coronary trees derived from CCTA were used only for display purposes and were not used in any way during the image registration process. The image registration algorithm was based on only the original transverse datasets.

CCTA-guided MPI contour and territory adjustment—At first, MPI images were evaluated blinded to the CCTA result and without fusing CCTA images. Then, fused CCTA and MPI images were evaluated with overlaid contours in multiplanar orientations (both cardiac axis and orthogonal views) in the fusion page of the QPET program. If discrepancies between the MPI valve plane position and the location on CCTA were seen on the fused images, the contour was manually adjusted in the standard manual QPET page with standard Mask and Constrain options(20); subsequently, the adjusted PET contour was verified by the CCTA fusion. Next, the default vascular territory boundaries were overlaid with the 3D LV MPI surfaces, with color-coded perfusion information and with a co-registered volume rendered segmented 3D coronary tree as described above. Vascular territories could then be adjusted segment by segment (based on a 17-segment American Heart Association model), using anatomic information provided by the 3D visualization of coronary vessels superimposed with MPI surfaces.

Statistical Analysis

All continuous variables are expressed as mean ± SD. The overall agreement in all directions was determined by calculating the linear weighted kappa coefficient between 2 observers, between each observer versus the automated software and between averages of 2 observers against automated software. The alignment tolerance of 5mm was applied between 2 observers, between observer and automated software. Similarly, the categorical scores for the kappa agreement have been computed by assuming 5 mm steps. The 95% limits of agreement from Bland-Altman analysis were reported and the McNemar's test was also performed. The inter-observer variability was computed in all 3 directions. Successful automated co-registration was defined as the result with an offset from mean observer location choice of   5 mm. Statistical analyses were performed with SPSS software (version 19.0, SPSS Inc., Chicago, Illinois).

RESULTS

Characterization of perfusion abnormalities on PET before fusion of PET MPI and CCTA are described in Table 2. Quantitatively, mean TPD was 11.7% ± 11.6% on stress and 5.1% ± 10.0% on rest. Myocardial ischemia and obstructive stenosis findings before fusion of PET MPI and CCTA are summarized in Table 3. The presence of obstructive stenosis on CCTA was noted in 13 of 32 studies, with 7 left anterior descending artery (LAD) lesions, 6 left circumflex artery (LCX) lesions and 6 right coronary artery (RCA) lesions. In the lesions with obstructive stenosis on CCTA, myocardial ischemia was found in 6 LAD lesions, 3 LCX lesions and 5 RCA lesions on PET MPI. In the lesions without obstructive stenosis, 17 out of 25 showed no ischemia in LAD, 22 out of 26 showed no ischemia in LCX, and 21 out of 26 showed no ischemia in RCA.

There was excellent agreement in all directions between 2 observers (97%), with a kappa value of 0.90 [95% confidence intervals (CI) 0.86 to 0.94, p <0.0001], McNemar's p=NS for rest. Similarly, there was excellent agreement between 2 observers (96%), with kappa value of 0.86 (95% CI 0.80 to 0.93, p <0.0001), McNemar's p=NS for stress. In regard to translations on rest, 95% limits of agreement from Bland-Altman comparison ranged from −0.6 to 0.8 mm with a low bias of 0.1 mm in x, −1.0 to 0.4 mm with a low bias of 0.3 mm in y and −1.4 to 0.7 mm with a low bias of 0.3 mm in z. Similar results were found for stress. The 95% limits of agreement ranged from −0.7 to 1.0 mm with a low bias of 0.1 mm in x, 0.0 to 1.8 mm with a low bias of 0.9 mm in y, and −0.1 to 1.3 mm with a low bias of 0.6 mm in z. In Table 4, inter-observer variability is specified in all 3 directions and the mean values were ≤2mm in all 3 directions.

The frequency and magnitude of the initial misalignment by automated co-registration on rest and stress studies are shown Figure 2. The initial PET-CCTA misalignment was 27.2 ± 11.8 mm in x, 13.3 ± 11.5 mm in y, and 14.3 ± 9.1 mm in z axes on rest (Figure 3A), 26.3 ± 10.2 mm in x, 11.1 ± 9.5 mm in y, and 11.7 ± 7.1 mm in z axes on stress (Figure 3B) studies. The frequency and magnitude of the initial misalignment by average of 2 observers (manual registration) on rest and stress studies are shown Figure 4. The initial PET-CCTA misalignment by average of 2 observers (manual registration) was 26.4 ± 11.2 mm in x, 12.6 ± 10.8 mm in y, and 11.2 ± 8.3 mm in z axes on rest (Figure 5A), 25.3 ± 11.0 mm in x, 10.1 ± 8.5 mm in y, and 8.3 ± 6.4 mm in z axes on stress (Figure 5B) studies.

As shown in Table 5, there was excellent agreement in all directions between each observer versus automated software. Automated PET-CCTA co-registration had excellent agreement against mean of observers [agreement 97%, kappa (95% CI) 0.83 (0.78 to 0.88), p <0.0001, McNemar's p=NS for rest; agreement 94%, kappa (95% CI) 0.80 (0.75 to 0.86), p <0.0001, McNemar's p=NS for stress]. The automated co-registration processing time was about 2 seconds for each case. The offset from mean observer location choice was 1.6 ± 1.2 mm in x, 2.3 ± 2.1 mm in y, and 3.7 ± 2.8 mm in z axes on rest, 2.4 ± 2.6 mm in x, 2.4 ± 2.3 mm in y, and 4.1 ± 2.9 mm in z axes on stress studies (Table 6). In regard to translations on rest, 95% limits of agreement from Bland-Altman comparison ranged from −1.4 to 0.1 mm with a low bias of −0.6 mm in x, −1.2 to 1.1 mm with a low bias of 0.0 mm in y and −4.7 to −2.6 mm with a low bias of −3.7 mm in z. Similarly, on stress, 95% limits of agreement ranged from −2.2 to 0.3 mm with a low bias of −1.0 mm in x, −1.1 to 1.3 mm with a low bias of 0.1 mm in y and −5.2 to −3.1 mm with a low bias of −4.1 mm in z.

Overlaid PET/CCTA trees were superimposed on the 3D MPI surface based on the automatic registration results between PET and CCTA volume. The coronary tree did not need to be adjusted for the display in any patient as qualitatively judged by both observers. Based on the 3D fusion of CCTA and PET, LV contours were adjusted in 8 studies and vascular territories were adjusted in another 3 studies with co-registered CCTA images as a guide. Myocardial ischemia and obstructive stenosis findings after fusion of PET MPI and CCTA are summarized in Table 7. In the lesions with obstructive stenosis on CCTA, myocardial ischemia was found in 6 LAD lesions, 4 LCX lesions and 5 RCA lesions on PET MPI. In the lesions without obstructive stenosis, 23 out of 25 showed no ischemia in LAD, 25 out of 26 showed no ischemia in LCX, and 23 out of 26 showed no ischemia in RCA. We could reduce false positive results by PET MPI resulting improved specificity (from 68/85/81% to 92/96/88% for LAD/LCX/RCA, respectively) and positive predictive value (from 43/43/50% to 75/80/63% for LAD/LCX/RCA, respectively) using CCTA as the reference standard.

Figure 6 shows an example of 3D visualization of coronary vessels superimposed with MPI surfaces before and after automated co-registration of MPI and CCTA. From the same

patient in Figure 7, we show an example of the fused images obtained by the automated co-registration of MPI with CCTA.

DISCUSSION

Hybrid SPECT-CCTA(21) or PET-CCTA imaging(22–24) performed in one session has been proposed for PET/CT scanners equipped with multidetector-CT. However, if MPI-CCTA scans are obtained on a hybrid scanner, even with data from both modalities in similar anatomic positions, interactive software realignment are required because of mismatches in the respiratory phases.(17, 21, 25) It is likely that the availability of fast and reliable automatic registration will allow routine review of fused MPI-CCTA in clinical practice whenever both datasets are available. The manual registration would have to be repeated separately for stress and rest scans, and perhaps other scans such as gated scans. Furthermore, the need for the manual interactive alignment of the images from two modalities introduces subjective errors and inter-observer variability, and limits the practical day-to-day clinical use of such tools. Therefore, we can save the physician's time and improve the overall clinical workflow of multimodality hybrid imaging by the use of such automated tools.

Although in the current study PET-CCTA was acquired on a hybrid scanner with the patient in the same bed position for both PET and CCTA scan, we have found that the average magnitude of the initial PET-CCTA misalignment was 27.2 ± 11.8 mm in x, 13.3 ± 11.5 mm in y, and 14.3 ± 9.1 mm in z axes on rest, 26.3 ± 10.2 mm in x, 11.1 ± 9.5 mm in y, and 11.7 ± 7.1 mm in z axes on stress studies. The initial misalignment is substantially larger than the offset from mean observer location choice or inter-observer variability. We have shown that automated software is very fast (2 seconds), reliable, and corrects for the initial misalignment just as visual observers do. The offset from mean observer location choice is comparable to the inter-observer variability. The agreement between the automated software and the visual observers is similar to the agreement between 2 observers. We demonstrated that our automated co-registration method has a success rate of 95% in eliminating the initial PET-CCTA misalignment, with a similar offset from mean observer location choice as achieved in our previous study of CCTA-SPECT registration.(6)

In our previous method for SPECT-CCTA registration, gated images were processed with a motion-frozen algorithm(26) or phase matching(7) in order to provide static myocardial perfusion SPECT images to match the cardiac phase of CCTA.(6) In the current study, we did not use motion-frozen data to demonstrate the practical image of image fusion with static perfusion data used in routine clinical analysis. Further evaluation could be performed with the motion-frozen data and phase matching, and may yield more accurate results for both visual observers and the automatic algorithm.

Finally, we have shown that the fusion approach synergistically improves the identification of obstructive stenosis using CCTA as the reference standard, especially in specificity and positive predictive value and no loss in sensitivity or negative predictive value.

Limitations

This study has several limitations. First, our sample of studied patients is relatively small. Then the results of invasive coronary angiography (as the gold standard for evaluation of coronary stenosis) were not available in this study since only a small proportion of the patients underwent this procedure. Nevertheless, this study focused on the validation of the automated alignment between the 2 modalities. Although we performed fully automated image registration, the contour definitions and vascular territory were manually guided by the coregistered CCTA anatomy; however, it is feasible that this adjustment can be

automated in the future if automatic segmentation of CCTA scan is performed. In our application, the success of registration depends on successful MPS contour determination. If the contours are incorrectly determined, causing the LV shape to be grossly distorted, the automatic registration could fail. Further, it is a currently clinically uncommon occurrence for patients to have both PET and CCTA studies; however, such protocols have been proposed for certain patient groups.(27, 28) Our estimated mean effective radiation dose was similar with helical CT protocol in those previous reports. The hybrid approach used in this study was associated with a higher radiation exposure than alternative approaches using either PET or CCTA alone.(29) Note that the ^{13}N-ammonia scan dose is very low for both rest and stress scans (1.5 mSv for each)(9), which is much lower than radiation dose from the SPECT scan. Therefore dosimetry from the combined study ^{13}N-ammonia PET is comparable to approaches commonly used to investigate CAD (i.e., one-day technetium 99m SPECT and CCTA or invasive coronary angiography). This exposure will be greatly reduced, providing the ability of more extensive ECG dose modulation and prospective gating with step-and-shoot protocols, which is expected to greatly reduce radiation doses from CCTA by more than 50%. Furthermore, by potentially reducing the number of unnecessary coronary revascularization procedures, the hybrid approach will ultimately result in a lower overall radiation burden in patients. In addition, hybrid imaging may allow stress-only PET further reducing radiation dose.(28, 30) Finally, the motion-frozen data was not used and the phase on CCTA was not matched to MPI. This may be revisited in the future when "motion-frozen" images are used routinely for perfusion assessment.

CONCLUSIONS

Software co-registration of CCTA and PET obtained on hybrid PET/CT scanners is still necessary due to different breathing protocols with the two modalities, but it can be performed rapidly and automatically, allowing rapid integrated 3D display and CCTA-guided contour and territory adjustment on PET.

Acknowledgments

REFERENCES

1. Berman D, Hachamovitch R, Shaw L, Friedman J, Hayes S, Thomson L, et al. Roles of nuclear cardiology, cardiac computed tomography, and cardiac magnetic resonance: assessment of patients with suspected coronary artery disease. J Nucl Med. 2006; 47:74–82. [PubMed: 16391190]

2. Taylor AJ, Cerqueira M, Hodgson JM, Mark D, Min J, O'Gara P, et al. ACCF/SCCT/ACR/AHA/ ASE/ASNC/NASCI/SCAI/SCMR 2010 appropriate use criteria for cardiac computed tomography: a report of the American College of Cardiology Foundation Appropriate Use Criteria Task Force, the Society of Cardiovascular Computed Tomography, the American College of Radiology, the American Heart Association, the American Society of Echocardiography, the American Society of Nuclear Cardiology, the North American Society for Cardiovascular Imaging, the Society for Cardiovascular Angiography and Interventions, and the Society for Cardiovascular Magnetic Resonance. J Am Coll Cardiol. 2010; 56:1864–1894. [PubMed: 21087721]

3. Gaemperli O, Schepis T, Valenta I, Husmann L, Scheffel H, Duerst V, et al. Cardiac image fusion from stand-alone SPECT and CT: clinical experience. J Nucl Med. 2007; 48:696–703. [PubMed: 17475956]

4. Santana CA, Garcia EV, Faber TL, Sirineni GK, Esteves FP, Sanyal R, et al. Diagnostic performance of fusion of myocardial perfusion imaging (MPI) and computed tomography coronary angiography. J Nucl Cardiol. 2009; 16:201–211. [PubMed: 19156478]

5. Gaemperli O, Schepis T, Kalff V, Namdar M, Valenta I, Stefani L, et al. Validation of a new cardiac image fusion software for three-dimensional integration of myocardial perfusion SPECT and stand-alone 64-slice CT angiography. Eur J Nucl Med Mol Imaging. 2007; 34:1097–1106. [PubMed: 17245532]

6. Slomka P, Cheng V, Dey D, Woo J, Ramesh A, Van Kriekinge S, et al. Quantitative analysis of myocardial perfusion SPECT anatomically guided by coregistered 64-slice coronary CT angiography. J Nucl Med. 2009; 50:1621–1630. [PubMed: 19759104]

7. Woo J, Slomka PJ, Dey D, Cheng VY, Hong BW, Ramesh A, et al. Geometric feature-based multimodal image registration of contrast-enhanced cardiac CT with gated myocardial perfusion SPECT. Med Phys. 2009; 36:5467–5479. [PubMed: 20095259]

8. Aladl UE, Hurwitz GA, Dey D, Levin D, Drangova M, Slomka PJ. Automated image registration of gated cardiac single-photon emission computed tomography and magnetic resonance imaging. J Magn Reson Imaging. 2004; 19:283–290. [PubMed: 14994295]

9. Johansson L, Mattsson S, Nosslin B, Leide-Svegborn S. Effective dose from radiopharmaceuticals. Eur J Nucl Med. 1992; 19:933–938. [PubMed: 1308762]

10. Raff G, Abidov A, Achenbach S, Berman D, Boxt L, Budoff M, et al. SCCT guidelines for the interpretation and reporting of coronary computed tomographic angiography. J Cardiovasc Comput Tomogr. 2009; 3:122–136. [PubMed: 19272853]

11. Slomka PJ, Nishina H, Berman DS, Akincioglu C, Abidov A, Friedman JD, et al. Automated quantification of myocardial perfusion SPECT using simplified normal limits. J Nucl Cardiol. 2005; 12:66–77. [PubMed: 15682367]

12. Berman D, Kang X, Hayes S, Friedman J, Cohen I, Abidov A, et al. Adenosine myocardial perfusion single-photon emission computed tomography in women compared with men. Impact of diabetes mellitus on incremental prognostic value and effect on patient management. J Am Coll Cardiol. 2003; 41:1125–1133. [PubMed: 12679212]

13. Shaw LJ, Berman DS, Maron DJ, Mancini GB, Hayes SW, Hartigan PM, et al. Optimal medical therapy with or without percutaneous coronary intervention to reduce ischemic burden: results from the Clinical Outcomes Utilizing Revascularization and Aggressive Drug Evaluation (COURAGE) trial nuclear substudy. Circulation. 2008; 117:1283–1291. [PubMed: 18268144]

14. Nakazato R, Berman D, Dey D, Le Meunier L, Hayes S, Fermin J, et al. Automated quantitative Rb-82 3D PET/CT myocardial perfusion imaging: normal limits and correlation with invasive coronary angiography. J Nucl Cardiol. 2011 In press.

15. Slomka PJ, Alexanderson E, Jácome R, Jiménez M, Romero E, Meave A, et al. Comparison of Clinical Tools for Measurements of Regional Stress and Rest Myocardial Blood Flow Assessed with 13N-Ammonia PET/CT. J Nucl Med. 2012

16. Slomka P, Germano G, Kavanagh P, Javadi M, Berman D, Bengel F. Evaluation of a new automatic algorithm for quantification of ECG-gated 82Rb cardiac PET. J Nucl Med. 2009; 50(Suppl 2):1167.

17. Slomka PJ. Software approach to merging molecular with anatomic information. J Nucl Med. 2004; 45(Suppl 1):36S–45S. [PubMed: 14736834]

18. Busch S, Johnson TR, Nikolaou K, von Ziegler F, Knez A, Reiser MF, et al. Visual and automatic grading of coronary artery stenoses with 64-slice CT angiography in reference to invasive angiography. Eur Radiol. 2007; 17:1445–1451. [PubMed: 17180326]

19. Levin D, Aladl U, Germano G, Slomka P. Techniques for efficient, real-time, 3D visualization of multi-modality cardiac data using consumer graphics hardware. Comput Med Imaging Graph. 2005; 29:463–475. [PubMed: 15979844]

20. Germano G, Kavanagh PB, Slomka PJ, Van Kriekinge SD, Pollard G, Berman DS. Quantitation in gated perfusion SPECT imaging: the Cedars-Sinai approach. J Nucl Cardiol. 2007; 14:433–454. [PubMed: 17679052]

21. Rispler S, Keidar Z, Ghersin E, Roguin A, Soil A, Dragu R, et al. Integrated single-photon emission computed tomography and computed tomography coronary angiography for the assessment of hemodynamically significant coronary artery lesions. J Am Coll Cardiol. 2007; 49:1059–1067. [PubMed: 17349885]

22. Di Carli MF, Dorbala S, Hachamovitch R. Integrated cardiac PET-CT for the diagnosis and management of CAD. J Nucl Cardiol. 2006; 13:139–144. [PubMed: 16580946]

23. Namdar M, Hany TF, Koepfli P, Siegrist PT, Burger C, Wyss CA, et al. Integrated PET/CT for the assessment of coronary artery disease: a feasibility study. J Nucl Med. 2005; 46:930–935. [PubMed: 15937302]

24. Javadi M, Mahesh M, McBride G, Voicu C, Epley W, Merrill J, et al. Lowering radiation dose for integrated assessment of coronary morphology and physiology: first experience with step-and-shoot CT angiography in a rubidium 82 PET-CT protocol. J Nucl Cardiol. 2008; 15:783–790. [PubMed: 18984453]

25. Slomka PJ, Baum RP. Multimodality image registration with software: state-of-the-art. Eur J Nucl Med Mol Imaging. 2009; 36(Suppl 1):S44–S55. [PubMed: 19104803]

26. Slomka P, Nishina H, Berman D, Kang X, Akincioglu C, Friedman J, et al. "Motion-frozen" display and quantification of myocardial perfusion. J Nucl Med. 2004; 45:1128–1134. [PubMed: 15235058]

27. Di Carli MF, Dorbala S, Curillova Z, Kwong RJ, Goldhaber SZ, Rybicki FJ, et al. Relationship between CT coronary angiography and stress perfusion imaging in patients with suspected ischemic heart disease assessed by integrated PET-CT imaging. J Nucl Cardiol. 2007; 14:799–809. [PubMed: 18022106]

28. Kajander S, Joutsiniemi E, Saraste M, Pietilä M, Ukkonen H, Saraste A, et al. Cardiac positron emission tomography/computed tomography imaging accurately detects anatomically and functionally significant coronary artery disease. Circulation. 2010; 122:603–613. [PubMed: 20660808]

29. Einstein AJ, Moser KW, Thompson RC, Cerqueira MD, Henzlova MJ. Radiation dose to patients from cardiac diagnostic imaging. Circulation. 2007; 116:1290–1305. [PubMed: 17846343]

30. Husmann L, Herzog BA, Gaemperli O, Tatsugami F, Burkhard N, Valenta I, et al. Diagnostic accuracy of computed tomography coronary angiography and evaluation of stress-only single-photon emission computed tomography/computed tomography hybrid imaging: comparison of prospective electrocardiogram-triggering vs. retrospective gating. Eur Heart J. 2009; 30:600–607. [PubMed: 19106197]
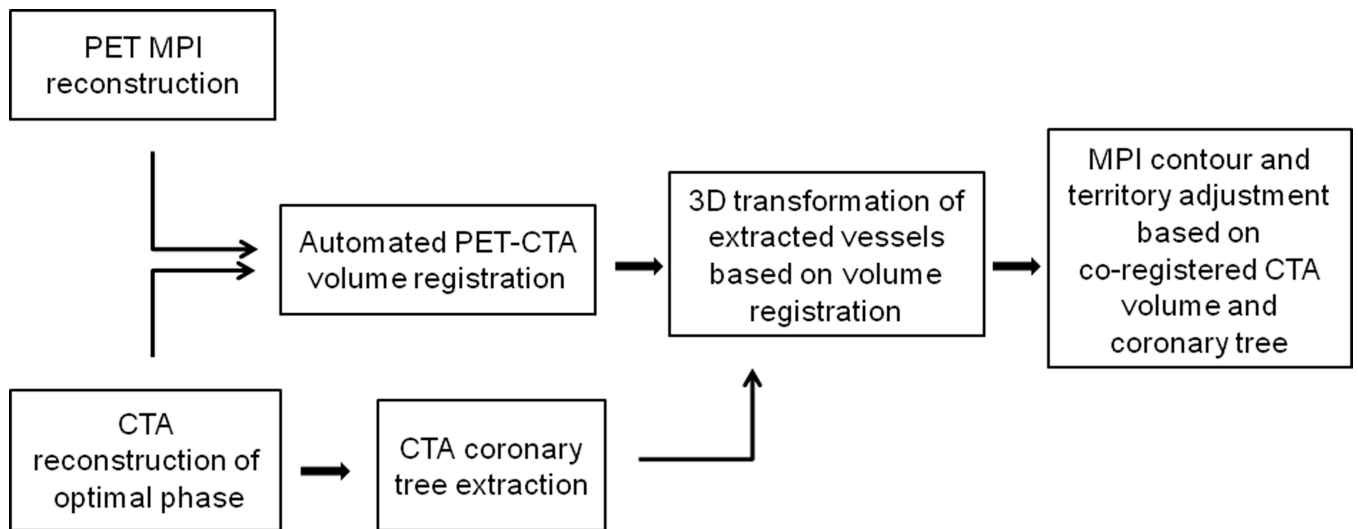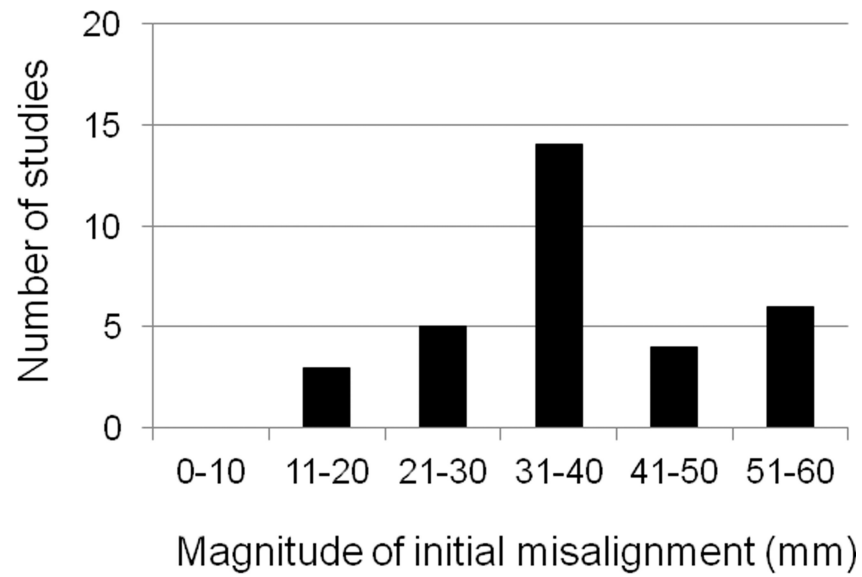
Figure 1.
Overview of image processing. CCTA = CT angiography.
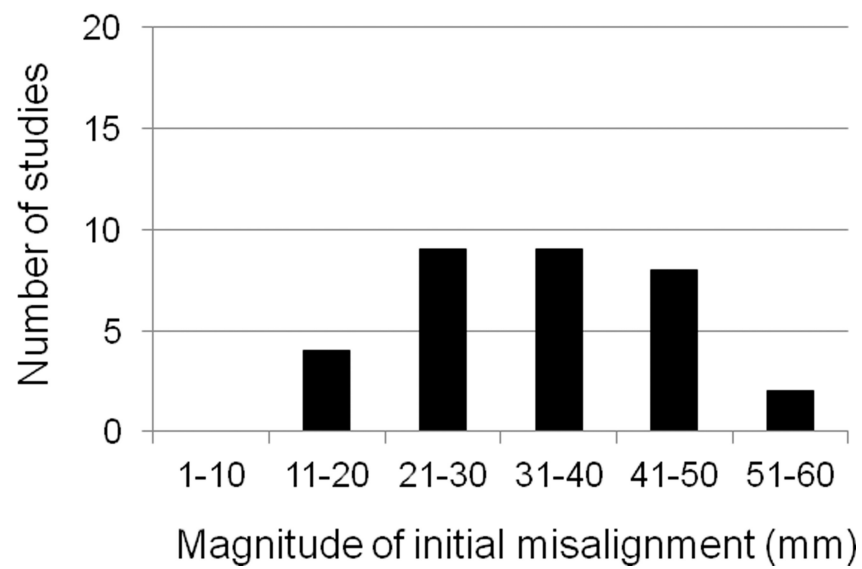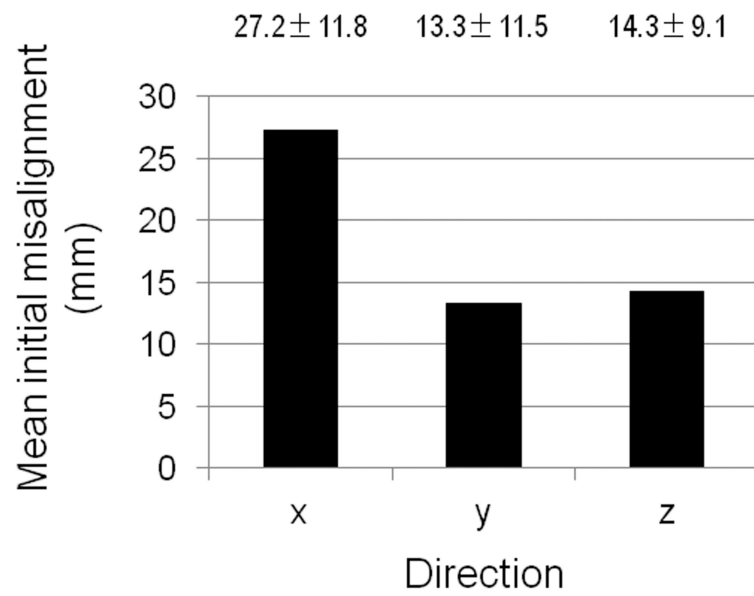
A   Rest

B   Stress

Figure 2.
Frequency and magnitude of the initial PET-CCTA misalignment on rest (A) and stress (B) studies by automated co-registration.

A Rest

27.2 ± 11.8   13.3 ± 11.5   14.3 ± 9.1

B Stress

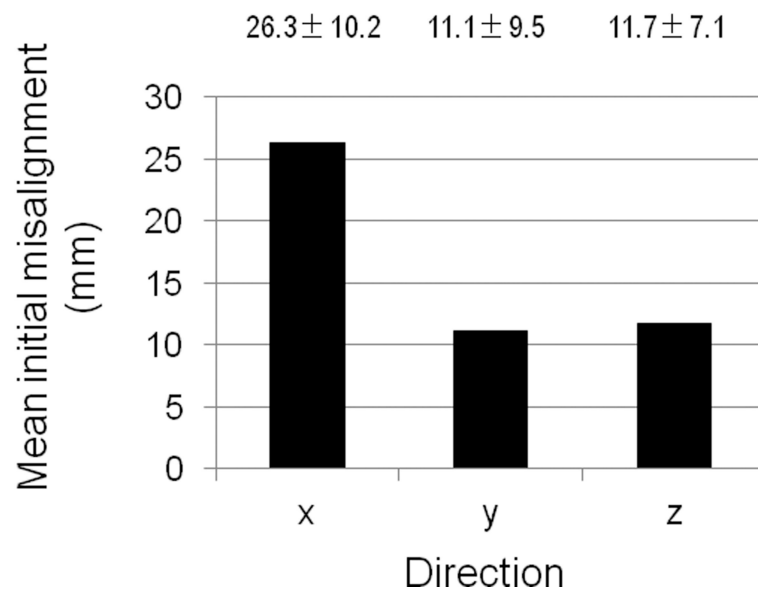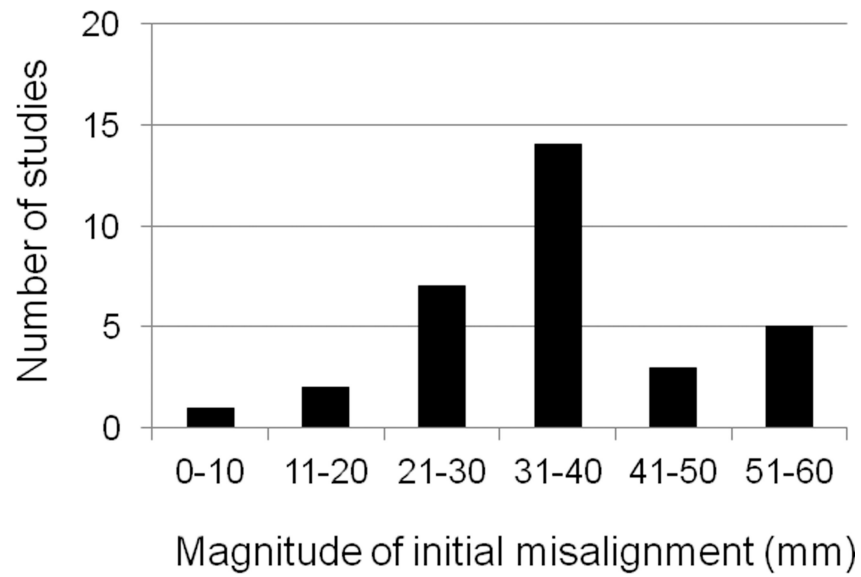26.3 ± 10.2   11.1 ± 9.5   11.7 ± 7.1

Figure 3.
Initial PET-CCTA misalignment by automated co-registration in each direction.

A Rest

B Stress

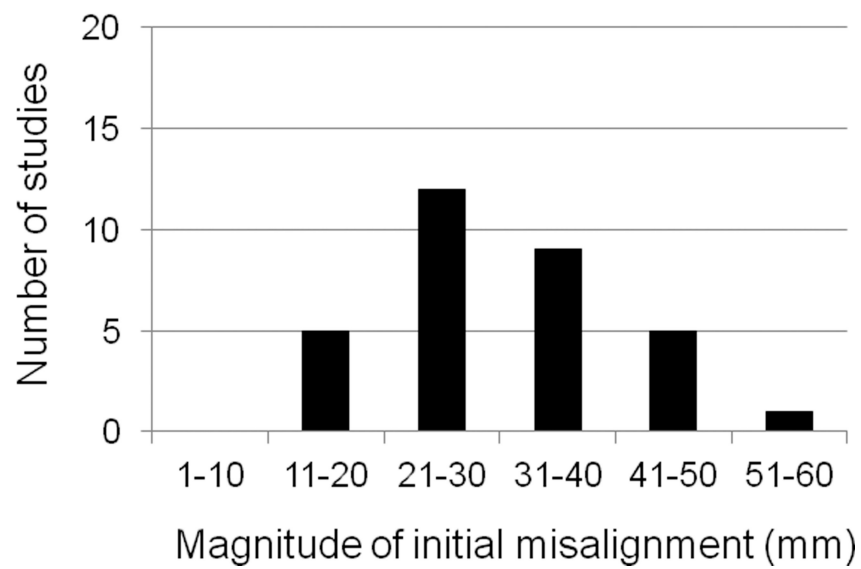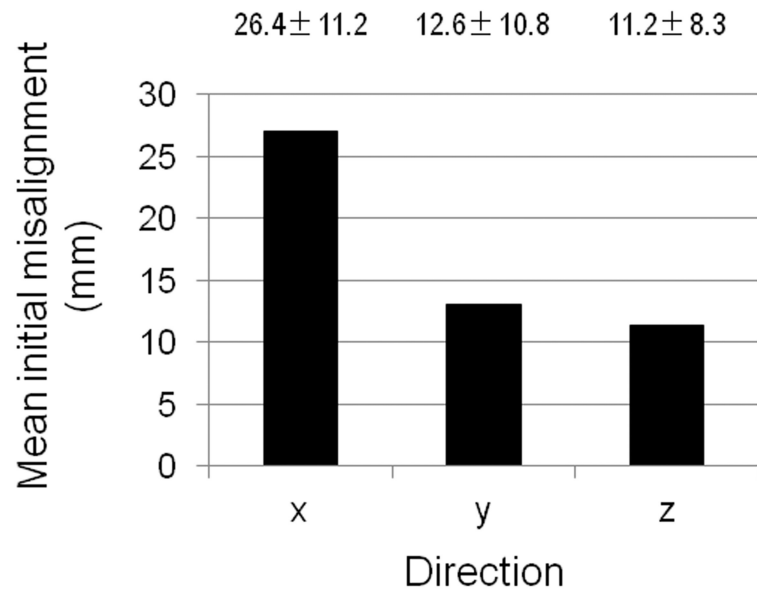**Figure 4.**
Frequency and magnitude of the initial PET-CCTA misalignment on rest (A) and stress (B) studies by manual registration.

A Rest

26.4± 11.2   12.6± 10.8   11.2± 8.3

B Stress

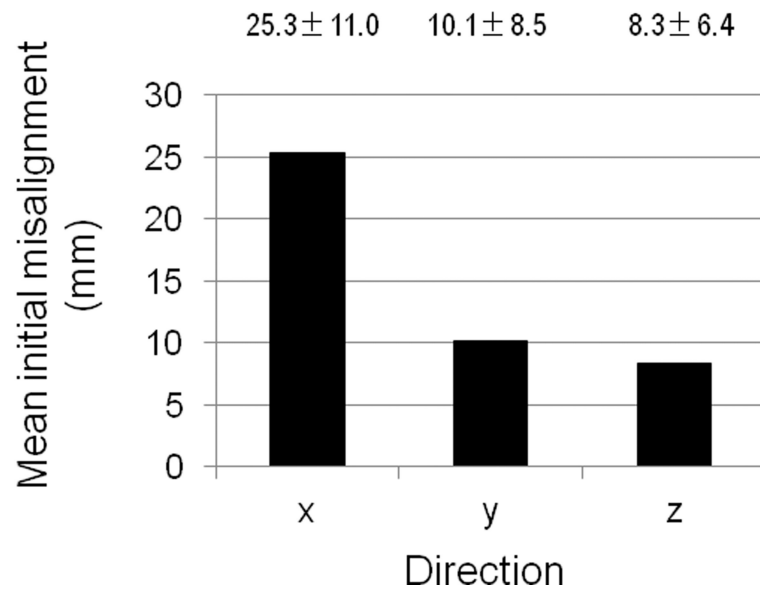25.3± 11.0   10.1± 8.5   8.3± 6.4

Figure 5.
Initial PET-CCTA misalignment by manual registration in each direction.
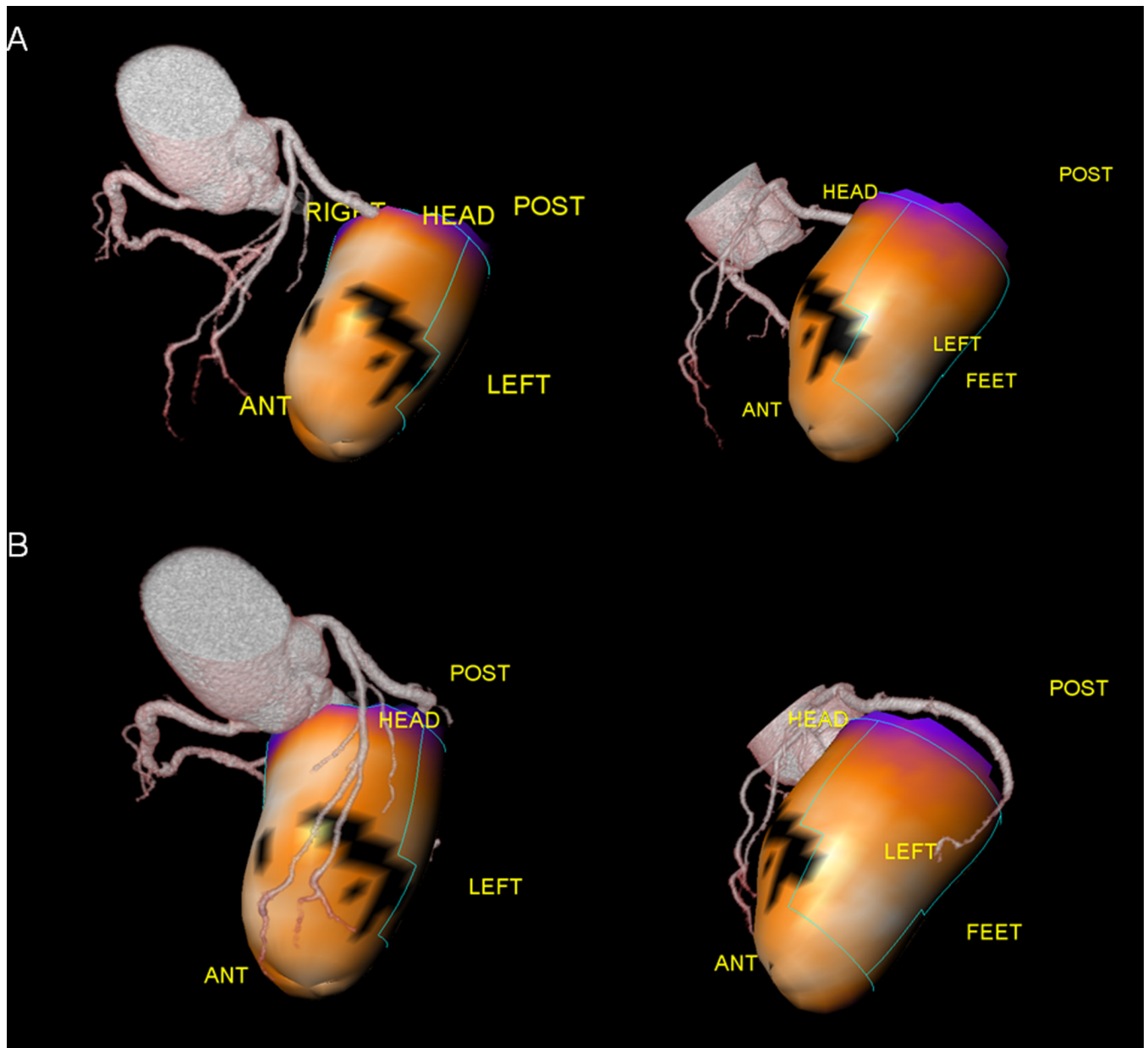
Figure 6.
3D visualization of coronary vessels superimposed with MPI surfaces, before and after CT misalignment correction.

Figure 7.
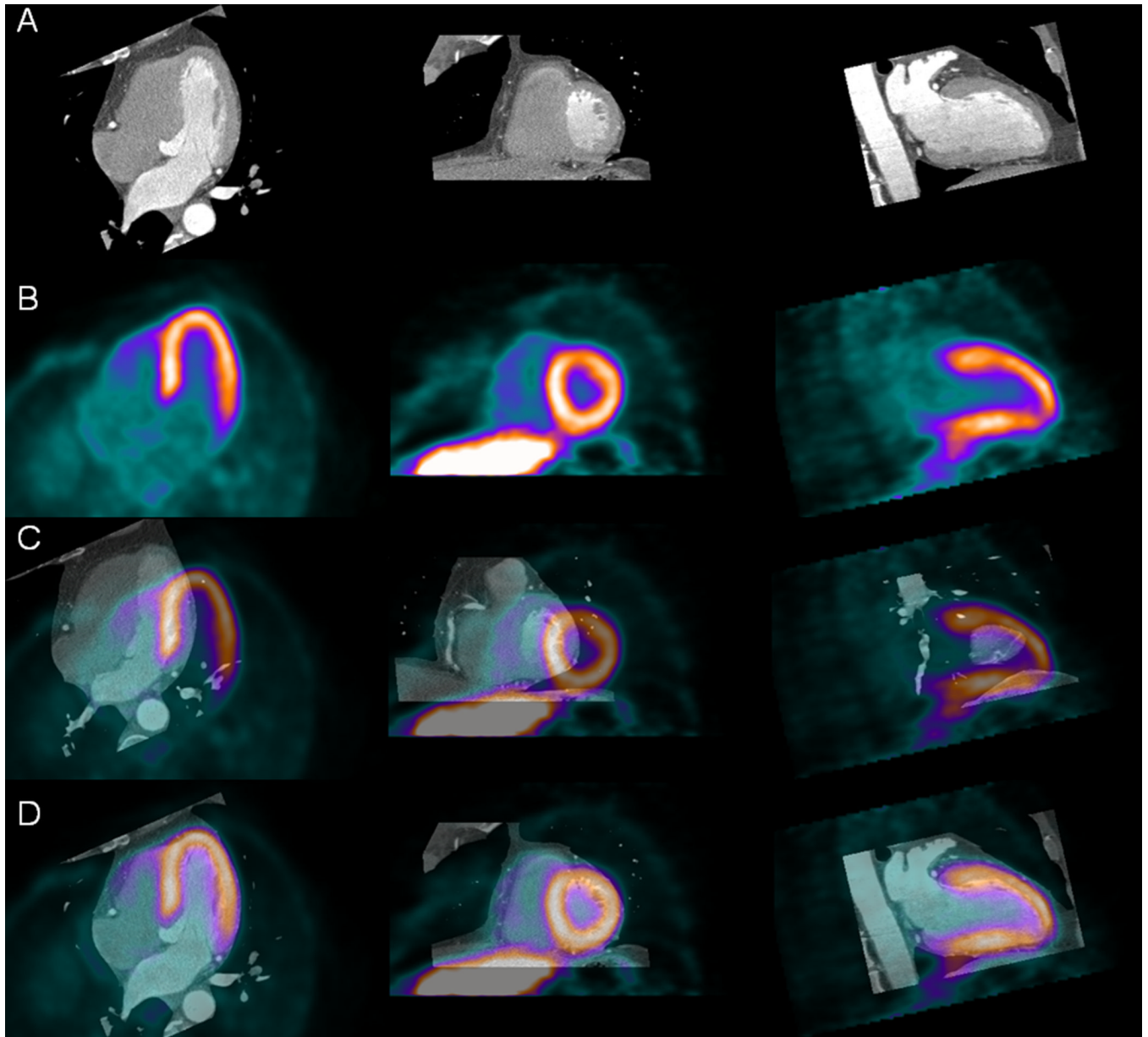Automated volume alignment of CCTA and MPI in same patient with Figure 6. Rows from top to bottom show in Multiplanar orientations original CCTA images (A), original MPI images (B), fused unregistered MPI and CCTA images (C), and same images after automated volume registration (D). Subsequentary, 3D transformation parameters obtained from volume registration can be used to align associated coronary trees with MPI surfaces.

Table 1

Patient characteristics

	Mean value
Sex, Male	21 (66%)
Age (y)	62 ± 9
Chest pain	17 (53%)
Dyspnea	9 (28%)
Abnormal rest ECG	5 (16%)
Pre-operation	1 (3%)
Myocardial infarction	7 (22%)
Weight (kg)	76 ± 14
Body mass index	27.2 ± 3.4

Data are mean ± SD, or number followed by percentage in parentheses (n = 32). *ECG*, electrocardiogram.

Table 2

Perfusion findings before fusion of PET MPI

	Mean value (%)
Global	-
stress TPD	11.7 ± 11.6
rest TPD	5.1 ± 10.0
reversible TPD	6.5 ± 5.0
Regional	
LAD	-
stress TPD	6.2 ± 9.0
rest TPD	3.4 ± 7.8
reversible TPD	2.9 ± 3.1
LCX	-
stress TPD	2.2 ± 3.3
rest TPD	0.7 ± 1.8
reversible TPD	1.5 ± 2.4
RCA	-
stress TPD	3.6 ± 4.5
rest TPD	1.6 ± 3.4
reversible TPD	2.0 ± 2.6

MPI, myocardial perfusion imaging; *TPD*, total perfusion deficit; *LAD*, left anterior descending artery; *LCX*, left circumflex artery; *RCA*, right coronary artery.

Table 3

Ischemia and stenosis findings before fusion of PET MPI and CCTA

LAD	Stenosis on CCTA	No stenosis on CCTA
Ischemia on PET	6	8
No ischemia on PET	1	17
Sens/spec/ppv/npv = 86/68/43/94% (CCTA stenosis was considered as the reference)		
LCX	Stenosis on CCTA	No stenosis on CCTA
Ischemia on PET	3	4
No ischemia on PET	3	22
Sens/spec/ppv/npv = 50/85/43/88%		
RCA	Stenosis on CCTA	No stenosis on CCTA
Ischemia on PET	5	5
No ischemia on PET	1	21
Sens/spec/ppv/npv = 83/81/50/95%		

CCTA, coronary CT angiography; *sens*, sensitivity; *spec*, specificity; *ppv*, positive predictive value; *npv*, negative predictive value.

Table 4

Inter-observer variability in PET/CCTA translation and magnitude.

Study	Direction (mm)			Magnitude (mm)
	x	y	z	
Rest	1.5 ± 1.3	1.4 ± 1.3	1.7 ± 2.5	3.2 ± 2.5
Stress	1.8 ± 1.5	2.0 ± 1.8	1.5 ± 1.5	3.6 ± 2.2

Table 5

Agreement in all directions between each observer versus automated software.

	Agreement (%)	kappa (95% CI)	p value	McNemar's p value
Observer 1 versus automated				
Rest	95	0.82 (0.77–0.87)	< 0.0001	NS
Stress	94	0.77 (0.71–0.83)	< 0.0001	NS
Observer 2 versus automated				
Rest	95	0.83 (0.78–0.88)	< 0.0001	NS
Stress	93	0.77 (0.71–0.83)	< 0.0001	NS

Table 6

Offset from mean observer location choice in PET/CCTA translation and magnitude.

	Direction (mm)			Magnitude (mm)
Study	**x**	**y**	**z**	
Rest	1.6 ± 1.2	2.3 ± 2.1	3.7 ± 2.8	5.3 ± 2.8
Stress	2.4 ± 2.6	2.4 ± 2.3	4.1 ± 2.9	6.0 ± 3.5

Table 7

Ischemia and stenosis findings after fusion of PET MPI and CCTA

LAD	Stenosis on CCTA	No stenosis on CCTA
Ischemia on PET	6	2
No ischemia on PET	1	23
Sens/spec/ppv/npv = 86/92/75/96% (CCTA stenosis was considered as the reference)		
LCX	Stenosis on CCTA	No stenosis on CCTA
Ischemia on PET	4	1
No ischemia on PET	2	25
Sens/spec/ppv/npv = 67/96/80/93%		
RCA	Stenosis on CCTA	No stenosis on CCTA
Ischemia on PET	5	3
No ischemia on PET	1	23
Sens/spec/ppv/npv = 83/88/63/96%		